

Phases of Talbot patterns in angular self-imaging

HUGUES GUILLET DE CHATELLUS,^{1,2,*} ERIC LACOT,^{1,2} OLIVIER HUGON,^{1,2} OLIVIER JACQUIN,^{1,2}
NAÏMA KHEBBACHE,³ AND JOSÉ AZAÑA⁴

¹Université Grenoble-Alpes, LIPhy, Grenoble F-38000, France

²CNRS, LIPhy, Grenoble F-38000, France

³Laboratory of Photonics Systems and Nonlinear Optics, Institute of Optics and Fine Mechanics, University of Sétif, Sétif 19000, Algeria

⁴INRS-Energie, Matériaux et Télécommunications, Montréal, Québec H5A1K6, Canada

*Corresponding author: hugues.guilletdechatellus@ujf-grenoble.fr

Received 4 February 2015; revised 20 April 2015; accepted 21 April 2015; posted 21 April 2015 (Doc. ID 233989); published 18 May 2015

The original Talbot (self-imaging) effect is observed in the vicinity of a grating of slits shined with a plane wave, and results in periodic images of the initial diffraction pattern (integer Talbot effect) and the appearance of images with a periodicity reduced by an integer factor (fractional Talbot effect). Most of the studies on Talbot effect so far have focused on the distribution of the intensity of the diffracted light. However, the phases of the Talbot images, obtained in both the integer and fractional self-imaging cases, can be calculated in a closed form and display interesting auto-correlation properties. This paper reports what is, to the best of our knowledge, the first experimental investigation of the phases of Talbot images beyond the integer self-imaging case. We address the problem of experimental measurement of the phases of the Talbot images in the equivalent frame of the angular Talbot effect, a recently reported manifestation of the Talbot effect in the far field. The phases of the Talbot images are measured by far-field holography, and the obtained results are in excellent agreement with theoretical calculations. They also suggest the possibility of using the scheme for a precise “fractional ruler” aimed at distances’ measurements. © 2015 Optical Society of America

OCIS codes: (050.1950) Diffraction gratings; (070.6760) Talbot and self-imaging effects.

<http://dx.doi.org/10.1364/JOSAA.32.001132>

1. INTRODUCTION

Since its discovery in optical diffraction [1,2], the Talbot effect has been observed and interpreted in various domains of wave physics, including quantum mechanics and electromagnetism in general [3–5]. Whereas the original Talbot effect was first observed and explained in the spatial domain, it was later observed in the temporal domain [6,7] and in the dual Fourier domains of spatial and temporal frequencies (angular and spectral Talbot effects, respectively) [8,9]. The most appealing features of the Talbot effect involve the possibility of creating an exact replica of a given periodic pattern (self-imaging, or integer Talbot effect) or the division of the periodicity of the original pattern by an integer factor (fractional Talbot effect). This property has led to applications in both the spatial domain (optical lithography and micro-patterning [10]) and the temporal domain (generation of trains of light pulses with high repetition rate [6,7]). Essentially, the Talbot effect arises from the interference of waves with quadratic relative phases: in the original Talbot effect, the contributions of the individual slits of the grating to the intensity in the near field have a quadratic phase dependence in the paraxial approximation, while in the time domain, the Talbot effect arises typically in dispersive lines that imprint a

quadratic spectral phase on the propagating pulses: the curvature of the parabola of the phases sets directly the specific integer or fractional Talbot pattern that is observed at the system output. Most of the practical applications of the Talbot effect so far make use of the intensity pattern, and the phase properties have triggered relatively limited interest, except for the case of Talbot array illuminators (TAIs). TAIs take advantage of the possibility of generating a pure phase image from an amplitude grating and, vice versa, the possibility of creating an amplitude pattern from a pure phase grating [11–13]. In this context, the phases of the Talbot images have been studied theoretically, but the theoretical investigations have been restricted to a specific subset of fractional Talbot conditions [14]. Interestingly, the sequence of phases arising in fractional Talbot images correspond to the arguments of so-called Gauss sums which, in turn, possess interesting autocorrelation properties [15,16]. For instance, considering that the phases of Talbot patterns constitute a set of orthogonal phase codes, they have been proposed as an alternative to Hadamard matrices for phase-encoded holographic multiplexing storage in volume-holographic media [17].

Despite their intrinsic fundamental interest and strong potential for information coding and processing applications, to the best of our knowledge, no experimental measurements of

the phases of the Talbot images have been reported yet, except for certain integer Talbot self-images and the observation of phase anomalies and Gouy phase shifts in the Talbot carpet [18,19]. Moreover, since the original Talbot effect is essentially a near-field effect, the experimental investigation of the phases of the individual Talbot images can become quite challenging, requiring, for instance, the use of a high resolution interference microscope [19].

In this paper, we extend the state of the art on the Talbot effect by reporting a simple technique that enables a measurement of the phases of any fractional Talbot self-image. Practical limitations related to the intrinsic near-field nature of the conventional Talbot effect are overcome by carrying out the desired experimental characterization in an equivalent configuration, namely, using the recently introduced angular Talbot effect. This effect can be interpreted as the counterpart of the spatial Talbot effect in the dual domain of angular frequencies, i.e., observed in the far field [8]. The concept we use for the target phase measurements is derived from far-field holography, where the initial wavefront interferes with the Talbot image under analysis; then the resulting intensity is linked directly to the phase pattern of the Talbot image. As an additional consequence, our observations suggest a new concept for distance measurement using the employed interferometric scheme, referred to here as a “fractional ruler,” where the distance between a point source and the diffraction grating is directly measured on the interference pattern, precisely expressed in the form of a fraction of two integers.

The paper is structured as follows: in the first section, we recall theoretical results on the classical near-field Talbot effect and focus especially on the phase of the Talbot images. Subsequently, we outline the direct equivalence between the original (near-field) and angular (far-field) Talbot effects. In the third section, we present our measurement scheme of the phases of the angular Talbot images, and the experimental results, which are found to show an excellent agreement with our theoretical predictions.

2. THEORETICAL ASPECTS OF THE NEAR-FIELD TALBOT EFFECT

In this section, we briefly recall the theory of the original (spatial) Talbot effect. Such an effect can be observed in the problem of Fresnel diffraction of a monochromatic plane wave of wavelength λ by a grating of a large number of slits (N), ideally infinite along the direction y , and periodically separated by a distance equal to Λ along the direction of x . We extend the theoretical treatment given in [20] by taking into account the envelope transmission function over the slits of the grating, $t_{\text{env}}(x)$. We define $g(x)$ as the transmission of the grating over an elementary cell of the grating (i.e., $-\Lambda/2 < x < \Lambda/2$). The grating is located in the plane $z = 0$. Since the slits are infinite along y , the theoretical treatment can be restricted to the spatial variables x and z (diffraction distance).

A. Grating Transmission Function

The transmission function of the grating is given by

$$t(x) = t_{\text{env}}(x) \sum_n g(x - n\Lambda), \quad (1)$$

and equivalently by

$$t(x) = \int g(x') \sum_n t_{\text{env}}(n\Lambda) \delta(x - x' - n\Lambda) dx'. \quad (2)$$

Equation (2) is valid under the condition that the grating envelope function $t_{\text{env}}(x)$ is much slower than the individual grating aperture function $g(x)$, such that $t_{\text{env}}(x)$ is approximately constant along the individual grating aperture. Strictly, the angular frequency bandwidth of $t_{\text{env}}(x)$ must be much narrower than the angular frequency bandwidth of $g(x)$.

The Fourier transform (FT) of $t(x)$ is $T(k_x) = \int t(x) e^{ik_x x} dx$. Then

$$T(k_x) = G(k_x) \sum_n t_{\text{env}}(n\Lambda) e^{ink_x \Lambda}, \quad (3)$$

where $G(k_x)$ and $T_{\text{env}}(k_x)$ are the FTs of $g(x)$ and $t_{\text{env}}(x)$, respectively. Defining $K_0 = \frac{2\pi}{\Lambda}$, the Poisson summation formula writes

$$\sum_n t_{\text{env}}(n\Lambda) e^{ink_x \Lambda} = \sum_m T_{\text{env}}(k_x + mK_0), \quad (4)$$

where the multiplicative constant has been dropped, and, finally,

$$T(k_x) = G(k_x) \sum_m T_{\text{env}}(k_x + mK_0). \quad (5)$$

B. Electric Field in the Fresnel Approximation

Assuming that the incident plane wave propagates along z , the electric field diffracted by the grating at location (x, z) is proportional to the convolution product (represented by $*$) of the transmission function of the grating, by the impulse response function of free space. In the Fresnel approximation, the latter can be written as $h_z(x) = h_0 e^{-ik_z k_x^2/4\pi}$, where $h_0 = i/\lambda z e^{-ik_z}$ and $k = \frac{2\pi}{\lambda}$ [21]. In the spatial frequency domain, the transfer function of free space is $H_z(k_x) = H_0 e^{ik_z k_x^2/4\pi}$, where $H_0 = e^{-ik_z}$. Therefore,

$$E(x, z) \propto t(x) * h_z(x) = FT^{-1}(T(k_x)H_z(k_x)), \quad (6)$$

which leads to

$$E(x, z) \propto H_0 \int G(k_x) \sum_m T_{\text{env}}(k_x + mK_0) e^{\frac{i\lambda z k_x^2}{4\pi}} e^{-ik_z x} dk_x. \quad (7)$$

Consistently with the above mentioned condition, Eq. (7) can be simplified greatly under the assumption that the function $G(k_x)$ keeps approximately constant over the angular frequency bandwidth of $T_{\text{env}}(k_x)$. Moreover, the quadratic phase term $e^{\frac{i\lambda z k_x^2}{4\pi}}$ can also be approximated by $e^{i\pi\lambda z k_x^2/\Lambda^2}$ when $(m - 1/N)K_0 < k_x < (m + 1/N)K_0$ (m integer). Under these conditions, Eq. (7) can be expressed as follows:

$$E(x, z) \propto t_{\text{env}}(x) e^{-ik_z x} \sum_m G(mK_0) e^{i\pi\lambda z \frac{w^2}{\Lambda^2}} e^{-imK_0 x}. \quad (8)$$

The usual Talbot carpet is obtained by plotting $|E(x, z)|^2$ in the (x, z) plane from Eq. (8) (Fig. 1, top). Another similarly interesting manifestation of the Talbot effect is the plot of the phase carpet in the (x, z) plane (Fig. 1, bottom).

C. Observation of the Talbot Effect

We define the Talbot length as $z_T = \Lambda^2/\lambda$ and consider the intensity at a distance from the grating z equal to a fraction p/q of the Talbot length (p and q being coprime integers). Then

$$E\left(x, \frac{p}{q}z_T\right) \propto t_{\text{env}}(x)e^{-ik\frac{p}{q}z_T} \sum_m G(mK_0)e^{i\pi\frac{p}{q}m^2} e^{-imK_0x}. \quad (9)$$

We now follow the standard procedure for the analysis of the Talbot effect and define $\varphi(m) = \pi\frac{p}{q}m^2$ [20].

When the product pq is even, $\varphi(m+q) = \varphi(m)$, while when pq is odd, $\varphi(m+q) = \varphi(m) + \pi$. We regroup the terms having the same phase, modulo π , which leads to

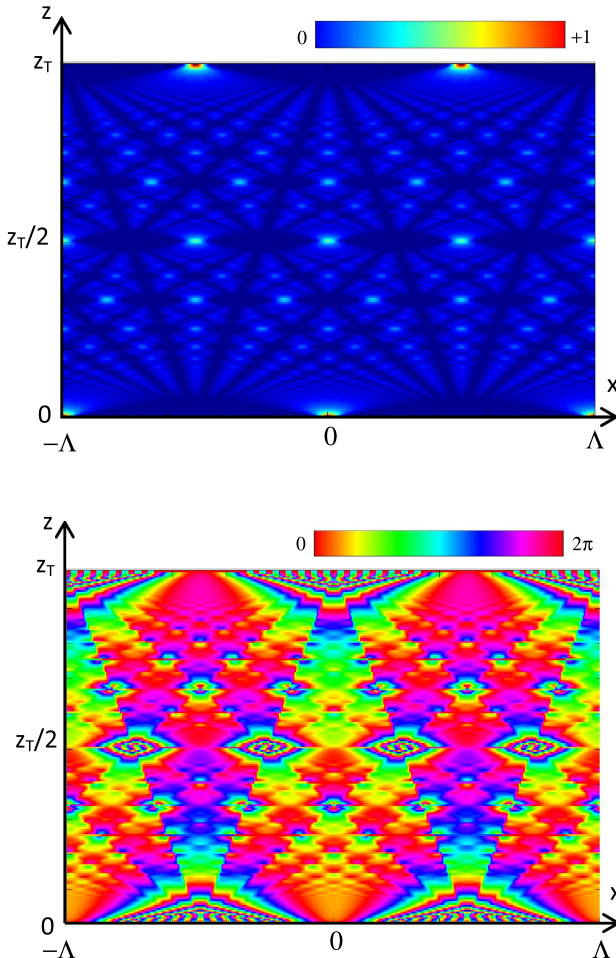


Fig. 1. Theoretical normalized intensity (top) and phase (bottom) Talbot carpets. A periodic grating of slits, centered at $x = 0$ and infinite along x , is shined with a plane monochromatic wave. The transmission function of the slits $g(x)$ is a Gaussian profile; the ratio between the width of the slits and the period of the grating is about 1/30. Top: intensity plot as a function of x and z when $-\Lambda < x < \Lambda$ and $0 < z < z_T$ (with $z_T = \Lambda^2/\lambda$). The intensity values are normalized with respect to the maximum across the pattern. Bottom: longitudinal differential phase because of the Talbot effect. The quantity $\arg(E(x, z)) - \arg(E_0(x, z))$ is plotted on the same boundary, $E_0(x, z)$ being the electric field of the incident plane wave that would have propagated in the absence of the grating, i.e., $E_0(x, z) \propto e^{-ikz}$. The asymmetric “hour-glass” shape at every Talbot spot (e.g., at $z = z_T/2$) is the signature of the Gouy phase in a one-dimensional geometry—or longitudinal $\pi/2$ -phase shift—as recently reported in [18].

$$\begin{aligned} E\left(x, \frac{p}{q}z_T\right) &\propto t_{\text{env}}(x)e^{-ik\frac{p}{q}z_T} \sum_{n=0}^{q-1} e^{i\pi\frac{p}{q}n^2} e^{-inK_0x} \\ &\times \sum_l G((n+lq)K_0)e^{-ilpq\pi} e^{-ilqK_0x}. \end{aligned} \quad (10)$$

Replacing G with its expression and dropping the first phase term gives

$$\begin{aligned} E\left(x, \frac{p}{q}z_T\right) &\propto t_{\text{env}}(x) \sum_{n=0}^{q-1} e^{i\pi\frac{p}{q}n^2} e^{-inK_0x} \int g(x') e^{inK_0x'} \\ &\times \sum_l e^{-ilqK_0(x-x')} e^{-ilpq\pi} dx'. \end{aligned} \quad (11)$$

The Poisson summation formula writes

$$\sum_l e^{-ilqK_0(x-x')} e^{-ilpq\pi} = \sum_l \delta\left(x' - x + \frac{\pi}{K_0}\left(\frac{2l}{q} - p\right)\right). \quad (12)$$

Finally,

$$\begin{aligned} E\left(x, \frac{p}{q}z_T\right) &\propto t_{\text{env}}(x) \sum_l g\left(x - \Lambda\left(\frac{l}{q} - \frac{p}{2}\right)\right) \\ &\times \sum_{n=0}^{q-1} e^{i\pi\frac{p}{q}pn^2 - 2nl + npq}. \end{aligned} \quad (13)$$

The Gauss sum defined by the second summation can be evaluated in closed form, depending on the parity of the integers p and q . It can be shown that

$$\sum_{n=0}^{q-1} e^{i\pi\frac{p}{q}pn^2 - 2nl + npq} = \sqrt{q} e^{i\Phi(l, q, p)}, \quad (14)$$

where the phasor $e^{i\Phi(l, q, p)}$ is given by the following expressions [22,23].

When p is even and q is odd,

$$\binom{p}{q} \exp\left(-i\frac{\pi}{4}\left[(q-1) + 4\frac{p}{q}\left(\left[\frac{1}{p}\right]_q\right)^2 l^2\right]\right). \quad (15)$$

When p is odd and q is odd,

$$\binom{p}{q} \exp\left(-i\frac{\pi}{4}\left[(q-1) + 8\frac{p}{q}\left[\frac{1}{2}\right]_q\left(\left[\frac{1}{2p}\right]_q\right)^2 (2l+q)^2\right]\right). \quad (16)$$

When p is odd and q is even,

$$\binom{q}{p} \exp\left(-i\frac{\pi}{4}\left[-p + \frac{p}{q}\left(\left[\frac{1}{p}\right]_q\right)^2 (2l+q)^2\right]\right). \quad (17)$$

Here, $\left[\frac{1}{a}\right]_b$ is the inverse of a modulo b and $\left(\frac{a}{b}\right)$ is the Jacobi symbol equal to +1 if there is an integer m so that $m^2 \equiv a[b]$ and -1 otherwise. Interestingly, the phases of the Talbot images show a quadratic dependence with the output individual aperture position, identified by the factor l . This is intimately linked to the fact that the Talbot images result from the interference of waves with quadratic relative phases and that the FT of a linear chirp (quadratic phase) is also a linear chirp.

D. Correlation Properties of the Phases of Talbot Images

Another interesting property of these phases appears when one considers the complex sequence defined by $r_l = e^{i\Phi(l,q,p)}$. The sequence is q periodic, and it can be shown that the autocorrelation of the sequence given by $c_n = \sum_{l=0}^{q-1} r_l r_{l+n}^*$ is equal to $q\delta(n \bmod q)$, where $\delta(n \bmod q)$ is equal to unity when n is a multiple of q , and 0 otherwise [16].

A simple physical proof can be given for this relation: since the Talbot image is the image of the grating after free space propagation in the near field, the intensity diffracted in the far field from the Talbot image is identical to the intensity diffracted in the far field by the initial grating. Considering a grating made of a large number of slits of negligible width and shined with a plane wave at normal incidence, the intensity diffracted in the far field is simply

$$I(k_x) \propto \sum_l \delta(k_x - lK_0) = \sum_n e^{i2\pi n k_x / K_0}. \quad (18)$$

The Wiener–Khinchin theorem for the intensity at $z = (p/q)z_T$ writes

$$I(k_x) \propto FT \left[E \left(x, \frac{p}{q} z_T \right) * E^* \left(x, \frac{p}{q} z_T \right) \right], \quad (19)$$

where we recall that $*$ stands for convolution. Straightforward calculations lead to

$$I(k_x) \propto \sum_n e^{i2\pi n k_x / q K_0} \sum_l r_l r_{l+n}^*. \quad (20)$$

The equivalence between Eqs. (18) and (20) implies that the autocorrelation $\sum_l r_l r_{l+n}^*$ vanishes except when n is a multiple of q . Therefore, the sequence of the phases occurring in the Talbot images is an example of delta-correlated discrete sequences, which have found applications in holography [17], acoustics, coding, and signal compression [15].

3. THEORETICAL DESCRIPTION OF THE FAR-FIELD (OR ANGULAR) TALBOT EFFECT

Despite their appealing properties, to the best of our knowledge, no experimental measurement of the phases of Talbot images has been provided yet, beyond the integer self-imaging case. One reason is that the classical Talbot effect is a near-field effect: indeed, any interferometric method requires mixing the Talbot image with a reference light beam, e.g., the incident light field, which implies a certain level of complexity [19].

Here we propose to measure the phases of the Talbot image by using a recently introduced, novel configuration, called “angular Talbot effect,” which involves an equivalent manifestation of the Talbot effect in the reciprocal spatial frequency domain [8]. The advantage over the classical Talbot effect is that it manifests in the far field, which inherently makes the investigation of the phases by a far-field holography technique more practical and flexible.

In the angular Talbot effect, the grating of slits is shined with a point-like light source located at a specific distance d from the grating. In the paraxial approximation, the phase profile of the wave that has propagated from the source to the plane of the grating has a parabolic (quadratic) shape. The intensity

diffracted in the far field by the grating (Fraunhofer approximation) results from the interference of waves with quadratic relative phase shifts, leading to a Talbot effect in the far field. More precisely, the angular Talbot effect can also be understood as a self-imaging effect in the dual space of transverse wave vector (or angular frequencies) [8]. The field diffracted in the far field by the grating shined with a point-like source is

$$\tilde{E}(k_x, k_y) \propto FT(t(x)h_d(x))e^{i\frac{2\pi}{\lambda}k_y^2}. \quad (21)$$

Interestingly, the x -dependent term $\tilde{E}(k_x) \propto FT(t(x) \cdot h_d(x))$ is simply the angular-frequency counterpart of Eq. (6). The derivation of the diffracted field is relatively straightforward: since the space variables x and y are separated, $\tilde{E}(k_x)$ can be evaluated in the plane $y = 0$.

The field at the grating location $(x, 0, 0)$ is proportional to

$$E(x, 0, 0) \propto t(x)h_d(x), \quad (22)$$

which leads to

$$E(x, 0, 0) \propto t_{\text{env}}(x) \int g(x') \sum_n \delta(x - x' - n\Lambda) e^{-i\frac{2\pi}{\lambda}n^2 \frac{\Lambda^2}{d}} dx' \quad (23)$$

and

$$E(x, 0, 0) \propto \int g(x') \sum_n \delta(x - x' - n\Lambda) t_{\text{env}}(n\Lambda) e^{-i\frac{2\pi}{\lambda}n^2 \frac{\Lambda^2}{d}} dx', \quad (24)$$

where we assume that the phase of the wave incident on the grating can be considered as a constant over the extension of a single slit. Note that the reference of the phases is taken at the slit #0 (i.e., at $x = 0$). The Fourier-transform of the electric field in the plane of the grating is

$$\tilde{E}(k_x) \propto G(k_x) \int \sum_n \delta(x - n\Lambda) t_{\text{env}}(n\Lambda) e^{-i\frac{2\pi}{\lambda}n^2 \frac{\Lambda^2}{d}} e^{ik_x x} dx. \quad (25)$$

Finally,

$$\tilde{E}(k_x) \propto G(k_x) \sum_n t_{\text{env}}(n\Lambda) e^{ink_x \Lambda} e^{-i\frac{2\pi}{\lambda}n^2 \frac{\Lambda^2}{d}}. \quad (26)$$

This result is mathematically equivalent to the form of Eq. (8), by properly exchanging the x and k_x variables, which allows one to draw a formal parallelism between the classical and the angular Talbot effect cases. By an analogy with the above discussions on the observation of the Talbot effect in the classical near-field case, the condition for the angular Talbot effect corresponds to a condition on the distance between the point-like source and the plane of the grating. In particular, when $d = \frac{m}{s}z_T$ ($z_T = \Lambda^2/\lambda$), m and s being coprime integers, the far-field diffraction pattern shows a multiplication of the diffraction orders (or division of the angular distance between consecutive diffraction orders) by a factor of m as compared to the case where the wave incident on the grating is a plane wavefront. More precisely, by directly transferring here the results obtained for the classical Talbot effect, when $d = \frac{m}{s}z_T$, the diffracted field is proportional to

$$\begin{aligned} \tilde{E}(k_x) &\propto G(k_x) \sum_l T_{\text{env}} \left(k_x - K_0 \left(\frac{l}{m} - \frac{s}{2} \right) \right) \\ &\times \sum_{n=0}^{m-1} e^{-i\frac{2\pi}{m}[sn^2 - 2nl + nms]}, \end{aligned} \quad (27)$$

which is again formally equivalent to Eq. (13). In particular, the phase of the wave diffracted along the transverse wave vector $k_x = K_0(\frac{l}{m} - \frac{s}{2})$ is simply $-\Phi(l, m, s)$. Using similar procedures to those outlined above for the classical Talbot effect, both intensity and phase carpets can be calculated in the angular case as well (Fig. 2). Notice that, despite the formal equivalence between near-field and angular Talbot effects, the carpets plotted on Figs. 1 and 2 differ because the angular Talbot carpets are plotted as a function of d , and not of $1/d$, which is the formal equivalent, in the angular case, of z in the near-field case.

4. MEASUREMENT OF THE PHASES IN THE TALBOT ANGULAR EFFECT

A. Principle

The possibility to observe the Talbot effect in the far field enables us to measure the phases of the Talbot pattern in a simpler

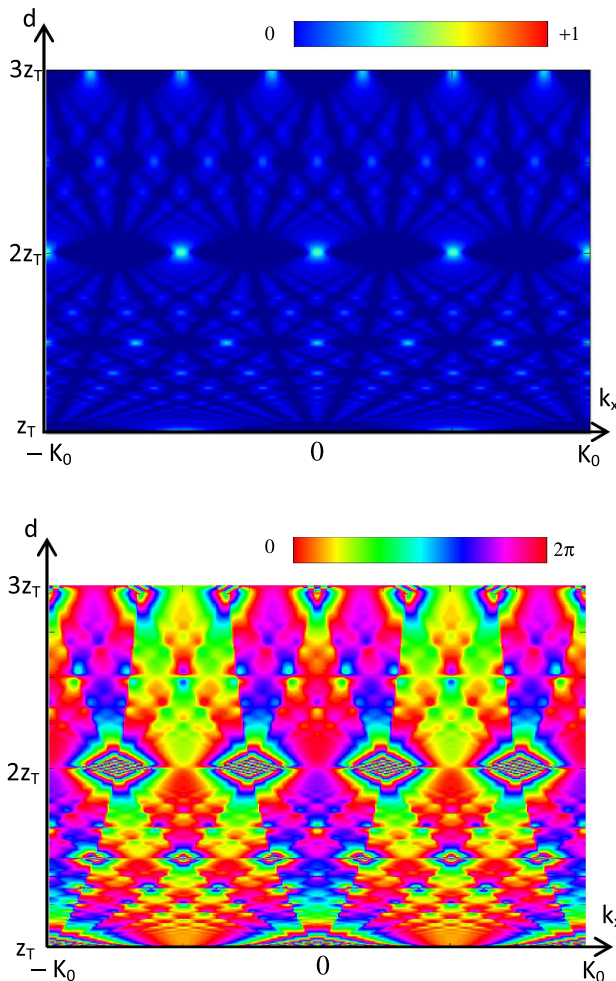


Fig. 2. Theoretical normalized intensity (top) and phase (bottom) angular Talbot carpets. A periodic grating of 51 slits, with negligible width and a Gaussian envelope transmission function centered at $x = 0$, is shined with a point-like source located at a distance d from the grating. Top: intensity plot as a function of k_x and d when $-K_0 < k_x < K_0$ and $z_T < d < 3z_T$ (with $z_T = \Lambda^2/\lambda$). Recall that if the grating were illuminated with a plane wave propagating along z , the light would be diffracted along the directions $k_x = nK_0$, n integer. Bottom: phase distribution in the angular Talbot effect (plot of $\arg(\tilde{E}(k_x))$).

manner since, in this case, it is relatively easier to “compare” the diffracted waves under analysis with a spherical reference wave, using a similar strategy to that of far-field holography [24]. We consider a grating of slits shined with a point-like source S located at a distance d from the grating.

A virtual reference point-like source S' coherent with the primary source S is vertically shifted from S , so that $SS' = a$. The field emitted by S' in the direction (k_x, k_y) at the object plane (distance d from the source) is given by

$$\tilde{E}_{\text{ref}}(k_x, k_y) \propto e^{i[a k_y + \frac{i d}{4\pi}(k_x^2 + k_y^2)]}, \quad (28)$$

where the reference of the phases is chosen at $\Omega(x = y = 0)$ (Fig. 3).

On the other hand, when the angular Talbot condition is satisfied, i.e., $d = \frac{m}{z_T}$ ($z_T = \Lambda^2/\lambda$), then the field diffracted by the grating in the direction (k_x, k_y) is, according to Eqs. (21) and (27),

$$\begin{aligned} \tilde{E}(k_x, k_y) &\propto G(k_x) \\ &\times \left(\sum_l T_{\text{env}} \left(k_x - K_0 \left(\frac{l}{m} - \frac{s}{2} \right) \right) e^{-i\Phi(l, m, s)} \right) e^{i\frac{ad}{4\pi} k_x^2}. \end{aligned} \quad (29)$$

When the amplitude of the reference wave matches the amplitude of the wave diffracted in the direction $(k_x = K_0(\frac{l}{m} - \frac{s}{2}), k_y)$, the resulting intensity of $\tilde{E}(k_x, k_y) + \tilde{E}_{\text{ref}}(k_x, k_y)$ is proportional to

$$1 + \cos \left(\Phi(l, m, s) + ak_y + \frac{1}{4\pi} \lambda d k_x^2 + \phi_0 \right), \quad (30)$$

where ϕ_0 is a constant phase shift. When the diffraction pattern is observed in the focal plane of a converging lens of focal length f , one obtains an image of the angular energy spectrum in Eq. (30), so that the coordinates (X, Y) of a point at the focal plane are linked to the transverse coordinates of the wave vector (k_x, k_y) by $X = \frac{\lambda f}{2\pi} k_x$ and $Y = \frac{\lambda f}{2\pi} k_y$. The aim of vertically shifting the virtual reference source is to record a continuous variation of the phase on the screen. It is worth noting that, even though the phases of the Talbot images are m periodic as a function of l , the recorded relative phase patterns are s periodic. This is because the described interferometric setup does not measure directly $\Phi(l, m, s)$: additional terms involving l , s , and m appear

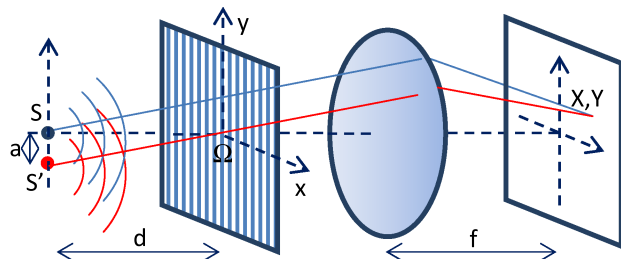


Fig. 3. Principle of the holographic measurement of the phases of the Talbot images in the configuration of the angular Talbot effect. The light diffracted by the grating of slits shined with the point-like source (blue) interferes with the reference (undiffracted) spherical wave produced by the virtual point-like source S' (red) in the far field (i.e., in the focal plane of a converging lens).

in Eq. (30), and it is simple to check that the resulting theoretical expression are in fact s periodic (Fig. 4). For instance, in the case where s is even and m is odd, the difference between the relative phases of Talbot images $l + s$ and l writes

$$\Delta\Phi = \Phi(l+s, m, s) - \Phi(l, m, s) + \pi \frac{m}{s} \left(\frac{l+s}{m} - \frac{s}{2} \right)^2 - \pi \frac{m}{s} \left(\frac{l}{m} - \frac{s}{2} \right)^2. \quad (31)$$

Then

$$\Delta\Phi = -2\pi \frac{ls^2}{m} \left(\left[\frac{1}{s} \right]_m \right)^2 - \pi \frac{s^3}{m} \left(\left[\frac{1}{s} \right]_m \right)^2 + 2\pi \frac{l}{m} - \pi s + \pi \frac{s}{m}, \quad (32)$$

which vanishes (modulo 2π). The calculation is similar for the two other cases.

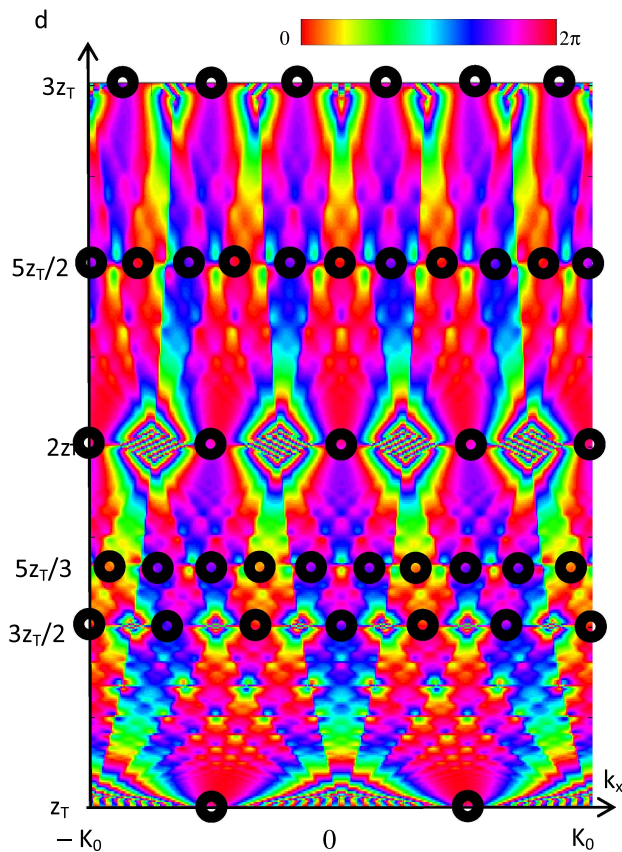


Fig. 4. Differential angular Talbot phase carpet: the quantity $\arg(\tilde{E}(k_x, 0)) - \arg(\tilde{E}_{\text{ref}}(k_x, 0))$ is plotted on the same boundary as Fig. 2. The grating is the same as in Fig. 2. The light diffracted in the far field interferes with the virtual spherical wave emitted by S (in this case $S' = S$). The black circles indicate the directions of the Talbot images in the cases $d = z_T, 3z_T/2, 5z_T/3, 2z_T, 5z_T/2$, and $3z_T$. Note that for any $d = mz_T/s$, the phases are s periodic, while the angular separation of the diffraction orders is divided by m (m and s being coprime integers).

B. Experimental Setup

The possibility to observe the Talbot effect in the far field renders the measurement of the phases of the Talbot images by interference techniques that are more practical and flexible. The experimental setup is a classical Mach–Zehnder interferometer tuned near optical contact. An He–Ne laser (wavelength $\lambda = 632.8$ nm) is sent into a microscope objective mounted on a translation stage. The resulting (spherical) wave is split and then recombined as in the usual Mach–Zehnder interferometer. A mirror in one of the arms is slightly tilted around the horizontal axis. Then the resulting interference pattern at the output of the interferometer observed at the focal plane of a converging lens (focal length f) consists in a succession of horizontal fringes with a fringe spacing equal to $\lambda f/a$, where a is the distance between the two secondary point-like sources induced by the tilt of the mirror, similarly to conventional Young's double hole experiment (Fig. 5, top). Then the grating of slits is inserted into the measurement arm of the interferometer (Fig. 5, bottom).

The grating is made with 50 slits (width: 7 μm) and the spatial period is $\Lambda = 70 \mu\text{m}$. The distance d between the point-like source and the grating can be adjusted by translating the grating. The intensity of the light pattern (hologram) is recorded on a CCD camera placed in the focal plane of the converging lens of focal length $f = 20$ cm. A rotating density filter (not shown in Fig. 5) enables the control of the intensity of the reference wave to maximize the contrast of the pattern recorded by the CCD camera. The distance d between the point source and the grating is set to match a fraction of the Talbot length (i.e., $d = \frac{m}{s}z_T$ where $z_T = 7.8$ mm). The results, shown in Fig. 6, demonstrate a good agreement with the theoretical predictions, illustrating the practicability and accuracy of the technique.

As predicted by the theoretical description of the angular Talbot effect, the angular separation of the diffracted beams (along the horizontal x direction) is inversely proportional to m . Interestingly, the intrinsic quadratic dependence of the phase profile of the Talbot image with l [Eqs. (15)–(17)] manifests by a parabolic shape of the interference pattern recorded on the CCD camera (especially visible in the cases $m/s = 6/5$ or $9/5$ in Fig. 6).

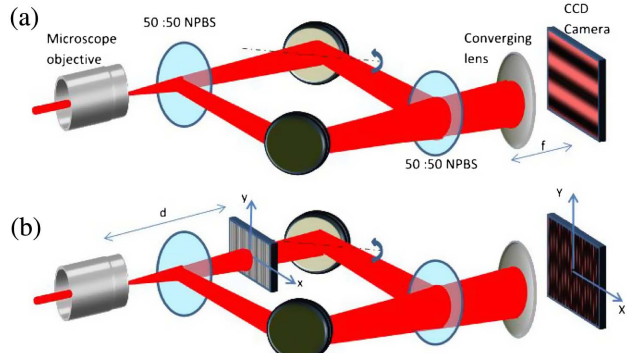


Fig. 5. Sketch of the experimental setup for the measurement of the phases of the Talbot images (see text). NPBS stands for non-polarizing beam-splitter.

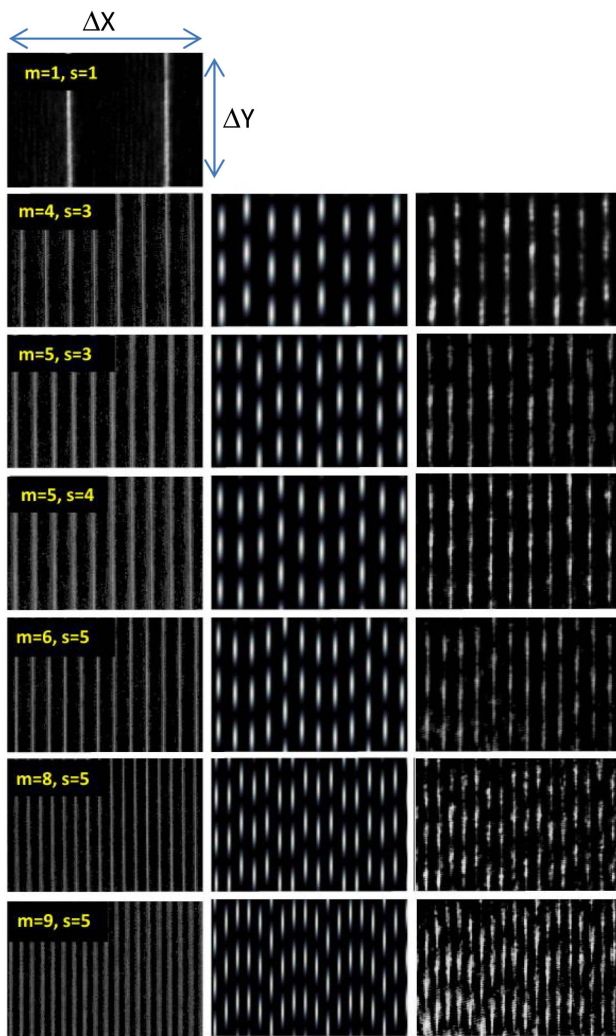


Fig. 6. Comparison between the theoretical and the experimental phase measurement for different values of d . Left column: experimental diffraction patterns in the angular Talbot effect (the reference arm is blocked). Middle (resp. right) column: theoretical (resp. experimental) phase images, or holograms. The size of the image recorded by the CCD camera in the focal plane of the converging lens corresponds to $\Delta Y = 3\lambda f/a$ in the vertical direction (i.e., $\Delta k_y = 6\pi/a$) and to $\Delta X = \lambda f K_0/\pi$ (i.e., $\Delta k_x = 2K_0$) in the horizontal direction. The contrast of both theoretical and experimental phase images has been numerically optimized for better visualization.

Finally, as predicted theoretically, the phase pattern measured with this method is s periodic. A surprising consequence of this property is that the values of m and s can be directly deduced from the two images recorded by the CCD, namely, from the multiplicative factor in the intensity diffraction pattern and from the periodicity of the interference pattern, respectively. Based on this observation, this setup can be interpreted as a “fractional ruler”: a precise fractional expression of the distance between the point source and the grating in units of z_T can be deduced directly from the recorded CCD images. This technique differs significantly from standard optical techniques for distance measurement, where the detected signal varies with the distance to be measured in a continuous manner. In contrast,

in the newly proposed method, diffraction pattern changes are observed in an entirely discrete fashion. Moreover, the result of the measurement is not a numerical value directly related to the distance of interest but consists of two coprime integers, whose ratio provides a precise estimate of the fractional distance to be measured—in units of the Talbot length.

5. CONCLUSION

In this paper, we have provided a detailed analysis of the parallelism between the original Talbot effect, which occurs in the near-field diffraction region of a grating shined with a plane wave, and the recently demonstrated angular Talbot effect, which is observed in the far field of a grating illuminated by a spherical wavefront. This analogy has allowed us to perform what we believe to be a first measurement of the phases of both integer and fractional Talbot images. Indeed, the angular Talbot effect offers a practical mean to carry out this measurement by far-field holography. Moreover, our results suggest the possibility of using the grating-based interferometry setup described here as a “fractional ruler,” capable of providing a direct, precise fractional expression of the distance between the point source and the grating. This novel, interesting concept represents another illustration of the fascinating features of the Talbot effect.

Commission Permanente de Coopération Franco-Québécoise; Énergie Matériaux Télécommunications-Institut National de la Recherche Scientifique; Institute of Optics and Fine Mechanics; Région Rhône-Alpes.

HGC acknowledges the Commission Permanente de Coopération Franco-Québécoise (Call for Grants PEES 2013), the Région Rhône-Alpes (Program C-MIRA Explora Pro 2014), and the EMT-INRS for their financial support. NK acknowledges the Institute of Optics and Fine Mechanics (Sétif, Algeria) for its financial support.

REFERENCES

- W. H. F. Talbot, “Facts relating to optical science. No. IV,” *Philos. Mag.* **9**(56), 401–407 (1836).
- Lord Rayleigh, “On copying diffraction gratings and on some phenomenon connected therewith,” *Philos. Mag.* **11**(67), 196–205 (1881).
- J. Wen, Y. Zhang, and M. Xiao, “The Talbot effect: recent advances in classical optics, nonlinear optics, and quantum optics,” *Adv. Opt. Photonics* **5**, 83–130 (2013).
- M. R. Dennis, N. I. Zheludev, and F. Javier Garcia de Abajo, “The plasmon Talbot effect,” *Opt. Express* **15**, 9692–9700 (2007).
- L. Deng, E. W. Hagley, J. Denschlag, J. E. Simsarian, M. Edwards, C. W. Clark, K. Helmerson, S. L. Rolston, and W. D. Phillips, “Temporal, matter-wave-dispersion Talbot effect,” *Phys. Rev. Lett.* **83**, 5407–5411 (1999).
- J. Azaña and M. A. Muriel, “Temporal self-imaging effects: theory and application for multiplying pulse repetition rates,” *IEEE J. Sel. Top. Quantum Electron.* **7**, 728–744 (2001).
- H. Guillet de Chatellus, O. Jacquin, O. Hugon, W. Glastre, J. Lacot, and E. Marklof, “Generation of ultra-high and tunable repetition rates in CW injection-seeded frequency shifted feedback lasers,” *Opt. Express* **21**, 15065–15074 (2013).
- J. Azaña and H. Guillet de Chatellus, “Angular Talbot effect,” *Phys. Rev. Lett.* **112**, 213902 (2014).

9. J. Azaña, C. Wang, and R. Chen, "Spectral self-imaging phenomena in sampled Bragg gratings," *J. Opt. Soc. Am. B* **22**, 1829–1841 (2005).
10. A. Isoyan, F. Jiang, Y. C. Cheng, F. Cerrina, P. Wachulak, L. Urbanski, J. Rocca, C. Menoni, and M. Marconi, "Talbot lithography: self-imaging of complex structures," *J. Vac. Sci. Technol. B* **27**, 2931–2937 (2009).
11. A. W. Lohmann and J. A. Thomas, "Making an array illuminator based on the Talbot effect," *Appl. Opt.* **29**, 4337–4340 (1990).
12. W. Klaus, Y. Arimoto, and K. Kodate, "Talbot array illuminators providing spatial intensity and phase modulation," *J. Opt. Soc. Am. A* **14**, 1092 (1997).
13. P. Szwajkowski and V. Arrizon, "Talbot array illuminator with multi-level phase gratings," *Appl. Opt.* **32**, 1109–1114 (1993).
14. C. Zhou and L. Liu, "Simple equations for the calculation of a multilevel phase grating for Talbot array illumination," *Opt. Commun.* **115**, 40–44 (1995).
15. M. R. Schroeder, *Number Theory in Science and Communications*, 5th ed. (Springer, 2009), Chap. 28.
16. H. Guillet de Chatellus, O. Jacquin, O. Hugon, and E. Lacot, "Theory of Talbot lasers," *Phys. Rev. A* **88**, 033828 (2013).
17. C. Zhou, S. Stankovic, C. Denz, and T. Tschudi, "Phase codes of Talbot array illumination for encoding holographic multiplexing storage," *Opt. Commun.* **161**, 209–211 (1999).
18. M.-S. Kim, T. Scharf, C. Menzel, C. Rockstuhl, and H. P. Herzig, "Phase anomalies in Talbot light carpets of self-images," *Opt. Lett.* **21**, 1287–1300 (2013).
19. M.-S. Kim, T. Scharf, C. Menzel, C. Rockstuhl, and H. P. Herzig, "Talbot images of wavelength-scale amplitude gratings," *Opt. Express* **20**, 4903–4920 (2012).
20. M. V. Berry and S. Klein, "Integer, fractional and fractal Talbot effects," *J. Mod. Opt.* **43**, 2139–2164 (1996).
21. B. E. A. Saleh and M. C. Teich, *Fundamentals of Photonics* (Wiley, 1991), Chap. 4.
22. H. C. Rosu, J. P. Treviño, and H. Cabrera, "Talbot effect for dispersion in linear optical fibers and a wavelet approach," *Int. J. Mod. Phys. B* **20**, 1860–1876 (2006).
23. S. Matsutani and Y. Onishi, "Wave-particle complementarity and reciprocity of Gauss sums on Talbot effects," *Found. Phys. Lett.* **16**, 325–341 (2003).
24. P. Hariharan, *Optical Holography: Principles, Techniques and Applications* (Cambridge University, 1996).